5*f*-electron states in uranium dioxide investigated using high-resolution neutron spectroscopy

G. Amoretti
Dipartimento di Fisica dell'Università degli Studi di Parma, Viale delle Scienze, I-43100 Parma, Italy

A. Blaise
Département de Recherche Fondamentale, Centre d'Études Nucléaires de Grenoble, Boîte Postale 85X, F-38041 Grenoble, France

R. Caciuffo*
European Institute for Transuranium Elements, Commission of the European Communities, P.O. Box 2340, D-7500 Karlsruhe 1, Federal Republic of Germany

J. M. Fournier
Département de Recherche Fondamentale, Centre d'Études Nucléaires de Grenoble, Boîte Postale 85X, F-38041 Grenoble, France

M. T. Hutchings
Materials Physics and Metallurgy Division, Harwell Laboratory, Didcot, Oxon OX11 0RA, United Kingdom

R. Osborn and A. D. Taylor
Neutron Science Division, Rutherford Appleton Laboratory, Chilton, Didcot, Oxon OX11 0QX, United Kingdom

(Received 16 January 1989)

High-resolution, high-energy-transfer, inelastic neutron scattering has been used to explore the crystal-field (CF) excitations in UO_2. As all the dipole-allowed transitions within the free-ion ground manifold have been identified, the observations provide a complete determination of the crystal-field potential and 5*f*-electron eigenstates. The fourth- and sixth-degree CF parameters are $V_4 = -123$ meV and $V_6 = 26.5$ meV. In spite of the strength of the CF, the ground state is accurately given by the intermediate-coupling approximation with little modification by *J*-mixing effects. In the antiferromagnetic phase below $T_N = 30.8$ K, a splitting of the cubic CF levels, due to the combined effects of the molecular field and the distortion of the oxygen-ligand cage surrounding the U^{4+} ions, has been observed. Detailed CF calculations are presented both for the case of a double-**k** magnetic structure with a monoclinic distortion of the oxygen sublattice, and for a combined triple-**k** distortion and magnetic order. The observed splittings are shown to be more consistent with the triple-**k** model.

I. INTRODUCTION

Uranium dioxide is one of the most frequently studied of all actinide compounds, attracting attention for both scientific and technological reasons. Fundamental questions concerning the nature of the 5*f* electrons, their degree of localization, the importance of covalency, and the strength of other interaction mechanisms have been explored in numerous experimental investigations.[1–4] In addition, the importance of UO_2 as a nuclear fuel has made its high-temperature thermodynamic properties the subject of detailed analysis.[5–9] The crystal field (CF) is an important component in all these studies. Because of the greater radial extent of the 5*f*-electron wave functions, the CF potential in actinide compounds is considerably stronger than in their lanthanide counterparts. In many instances, it may not be treated as a small perturbation on the ground state of the 5*f* configuration, but must be included on an equal footing with the intra-atomic interactions.[10] As a consequence, a knowledge of the CF potential is required in understanding both bulk and spectroscopic properties.

Neutron inelastic scattering provides a direct method of measuring the CF transition energies, but the first experiments on UO_2 have only recently been performed. The reason is that the energies of the first excited CF levels are above 100 meV, which is outside the range of most neutron scattering spectrometers. However, these energy transfers are readily accessible on the new generation of pulsed spallation neutron sources which have an enhanced epithermal component in their flux. The first direct measurements of the CF excitation energies using neutron scattering were made by Kern, Loong, and Lander[11] (KLL) at the Intense Pulsed Neutron Source (IPNS), Argonne National Laboratory. They observed two peaks, at 155 and 172 meV, with a resolution of 11 meV, both in the paramagnetic and antiferromagnetic phases. This was in contrast to earlier predictions of Rahman and Runciman[10] (RR) of one level at 169 meV, with the next level at 624 meV. KLL did not consider any of a number of possible explanations to be entirely satisfactory. The experiment has therefore been repeated at

the spallation neutron source ISIS, at the Rutherford Appleton Laboratory, with improved energy resolution and extending the energy range to cover the possible overall splitting of the free-ion ground manifold.

UO_2 is a semiconductor, crystallizing in the CaF_2 structure with $a_0=5.470$ Å at room temperature. The uranium ions are tetravalent with the $5f^2$ levels lying in a 6 eV gap between a valence band derived from oxygen $2p$ electrons and a conduction band derived from uranium $6d$ electrons.[1] As a consequence, the $5f$ electrons are well localized, and this is indicated experimentally by optical spectroscopy and photoemission results.[2] The effective Curie-Weiss paramagnetic moment is $\mu_{\text{eff}}=3.2\mu_B$, the paramagnetic temperature is $\Theta_P=-220$ K and the ordered magnetic moment, determined by neutron diffraction, is $\mu_0=1.74(2)\mu_B$.[3] The ground-state multiplet of the U^{4+} ion is $^3H_4$ within the Russell-Saunders (RS) coupling scheme. It is only slightly modified by intermediate-coupling (IC) effects which mix the $J=4$ manifolds belonging to different L-S terms.[1] However, the CF interaction, if sufficiently large, can give rise to a substantial mixing of states with different J. This makes the energies of the CF transitions extremely sensitive to the strength of the intra-$5f$ Coulomb and spin-orbit interactions, and so to the composition of the J-mixing wave functions. A determination of the CF-level scheme gives information not only on the strength of the CF potential, but also on the composition of the ground-state wave functions.

UO_2 exhibits a first-order phase transition at $T_N=30.8$ K to a type-I antiferromagnetic state associated with a Jahn-Teller distortion of the oxygen sublattice.[3] A double-**k** magnetic structure, with moments along $\langle 110\rangle$ directions and a single-**k** monoclinic lattice distortion, was initially proposed, but recent neutron-diffraction measurements under high magnetic field strongly favor a triple-**k** magnetic structure associated with a triple-**k** lattice distortion,[12] in which the uranium magnetic moments and oxygen displacements lie along the $\langle 111\rangle$ directions. In this paper these will be referred to as the double- and triple-**k** models, respectively. The measured neutron spectra below T_N show considerably more structure than those above. By comparing the experimental observations with detailed CF calculations, it is shown that this is a consequence of the splitting of the Γ_5, Γ_3, and Γ_4 CF levels by the combined effects of the molecular field and the distortion of the oxygen-ligand cage. The relative magnitudes of these splittings are quite different in the two models, so our results throw light on the ordered structure in the antiferromagnetic phase.

In Sec. II we outline the experimental methods employed, while in Sec. III we describe the experimental results. In Sec. IV the analysis of the observed CF transition energies in the paramagnetic phase is presented. A complete J-mixing diagonalization of Coulomb, spin-orbit, and cubic CF Hamiltonians has been performed in order to derive new cubic CF parameters. In Secs. V A and V B the effect on the cubic CF levels of the molecular field and lattice distortion of the double- and triple-**k** models, respectively, is calculated in the point-charge model (PCM) and intermediate-coupling approximation. There is a discussion of the results in Sec. VI with a summary of the conclusions in Sec. VII. Two preliminary reports of this work have already been published.[13,14]

II. EXPERIMENTAL DETAILS

The inelastic magnetic neutron scattering cross section from a system of N noninteracting ions, in the dipole approximation and for unpolarized neutrons, is given[15] by the polycrystalline average of

$$\frac{d^2\sigma}{d\Omega\, d\omega}=N(\gamma_N r_0)^2\frac{k_f}{k_i}e^{-2W}[\tfrac{1}{2}g_J f(Q)]^2 \times\sum_{n,m}p_n|\langle n|J_\perp|m\rangle|^2\delta(E_n-E_m-\hbar\omega)\,, \quad (1)$$

where γ_N is the neutron dipole moment in nuclear Bohr magnetons, r_0 is the classical electron radius, k_i and k_f are the incident and scattered neutron wave vectors, g_J is the Landé factor, e^{-2W} is the Debye-Waller factor, and $f(Q)$ is the $5f$-electron form factor [$f^2(Q)\simeq\exp(-0.07Q^2)$ with Q in Å^{-1}, for U^{4+} ions]. $|n\rangle$ and $|m\rangle$ are eigenfunctions of the CF Hamiltonian with eigenvalues E_n and E_m, respectively; $J_\perp$ is the component of the total-angular-momentum operator perpendicular to the scattering vector **Q**, and p_n is the occupation probability of $|n\rangle$. We use the conventional definition of scattering vector $\mathbf{Q}=\mathbf{k}_i-\mathbf{k}_f$ and energy transfer $\hbar\omega=E_i-E_f$, where E_i and E_f are the incident and scattered neutron energies. The inelastic neutron energy gain or loss spectrum is then composed of peaks corresponding to transitions allowed by magnetic dipole selection rules. The transition energies give the eigenvalues of the CF Hamiltonian, while their intensities provide information about the CF wave functions through the matrix elements of $J_\perp$ between the different states.

The Q dependence of the cross section allows magnetic and vibronic contributions to be distinguished since phonon scattering increases in intensity with Q, whereas magnetic scattering falls in intensity as $f^2(Q)$. This is an important advantage of the use of neutrons over optical

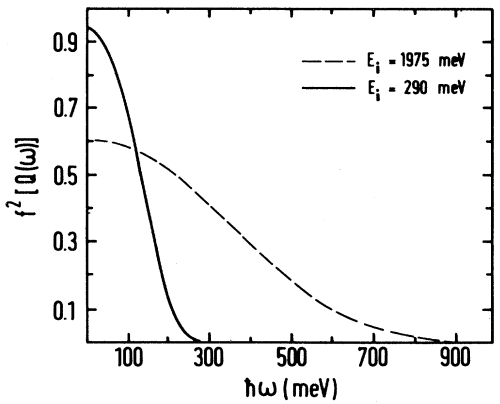

FIG. 1. Variation with the energy transfer $\hbar\omega$ of the square of the magnetic form factor for U^{4+} ions at a scattering angle of $\phi=5°$.

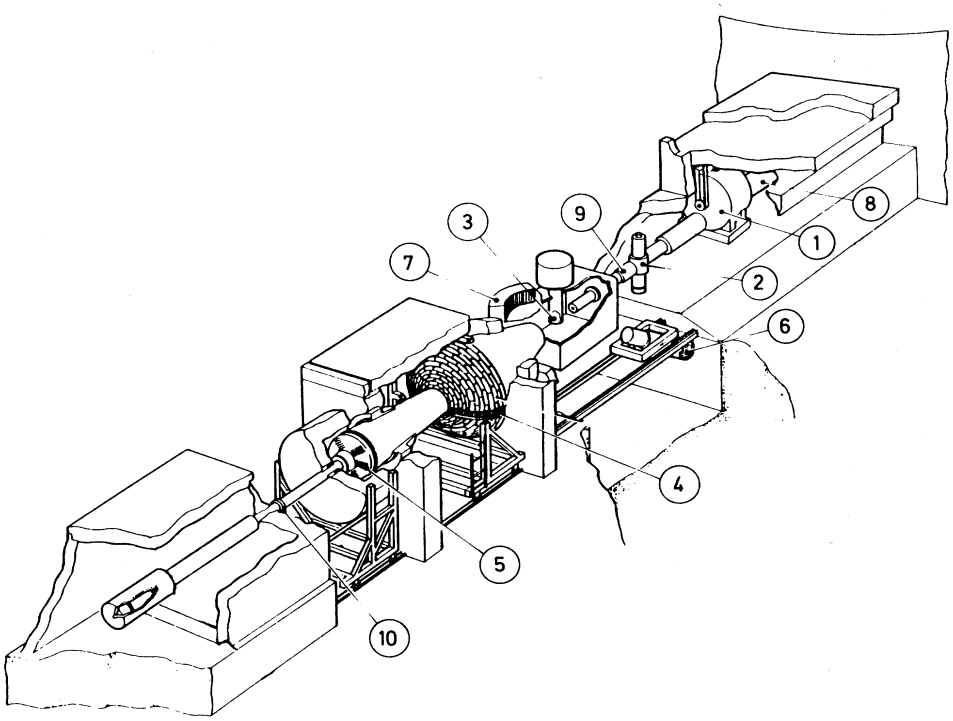

FIG. 2. Layout of the High Energy Transfer (HET) spectrometer at the ISIS spallation neutron source, showing the background-reducing (1) and monochromating (2) choppers, sample position (3), and the various detector arrays (4–7) and monitors (8–10); from Ref. 16.

spectroscopy, but it also means that CF transitions can only be measured at small values of momentum transfer. The kinematic constraints of a scattering process, expressed in the equation

$$\frac{\hbar^2 Q^2}{2m_N} = 2E_i - \hbar\omega - 2\cos\phi[E_i(E_i-\hbar\omega)]^{1/2} , \qquad (2)$$

where m_N is the neutron mass and ϕ the scattering angle, are particularly severe at high-energy transfers. In the limit $\phi \to 0$ the incident energy must be increased approximately as the square of the energy transfer to maintain a fixed value of Q. Figure 1 illustrates the penalty imposed by the form factor as the energy transfer increases for a fixed ϕ at two incident energies. Pulsed spallation neutron sources have a large flux of epithermal neutrons, with incident energies extending to greater than 1 eV, and are therefore particularly well suited to the study of magnetic excitations at energy transfers in the range 100–1000 meV.

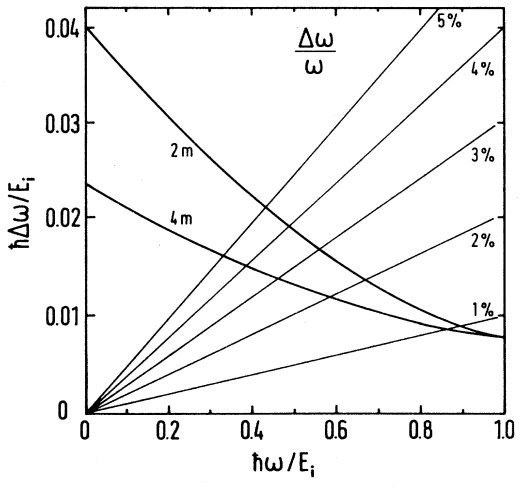

FIG. 3. Fractional energy-transfer resolution $\hbar\Delta\omega/E_i$ calculated for the 2- and 4-m detector banks of the HET spectrometer as a function of $\hbar\omega/E_i$, E_i being the incident energy. The values of $\hbar\omega/E_i$ necessary to obtain various percentages of $\Delta\omega/\omega$ are given by the intersections between the resolution curves and the straight lines.

The experiment was performed on the High Energy Transfer spectrometer (HET) at the U.K. spallation neutron source ISIS of the Rutherford Appleton Laboratory (RAL). HET is a direct-geometry chopper spectrometer,[16] shown as a schematic drawing in Fig. 2. A beam of monochromatic neutrons is produced at the sample by phasing a Fermi chopper, spinning at a frequency in the range 400–600 Hz, to the pulse of protons on the spallation target. Incident energies from 30 to 2000 meV may be selected by using different chopper slit packages, which optimize the transmission and match the chopper burst time to the intrinsic time resolution of the neutron pulse. The scattered neutrons are detected by two arrays of ^{3}He detectors, one lying at 4 m from the sample and covering a full scattering angle range $\phi = 3°$ to 7°, the oth-

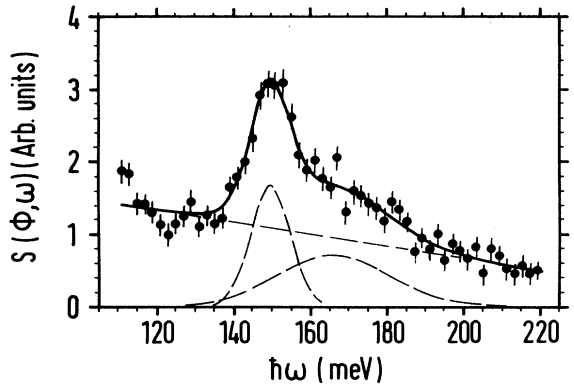

FIG. 4. Inelastic neutron scattering cross section measured in the paramagnetic phase of UO_2 at $T=50$ K, with an incident neutron energy of 290 meV. The energy transfer resolution is 3.6 meV at $\hbar\omega=160$ meV. The smooth line is the fit to two Gaussian line shapes and a sloping background. These three components are shown by the dashed lines.

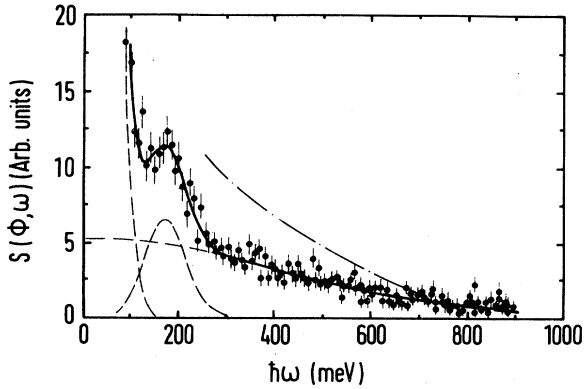

FIG. 5. Cross section of inelastic scattering of neutrons from UO_2 at 40 K with an incident energy of 1975 meV ($\Delta\hbar\omega=35$ meV at 500 meV). The dashed-dotted line gives the estimated height of the $\Gamma_5\rightarrow\Gamma_4$ peak as a function of energy, assuming the peak at 160 meV arises entirely from the $\Gamma_5\rightarrow\Gamma_3$ transition.

er being at 2.5 m from the sample and spanning the angular range between 10° and 30°. The former gives high-energy resolution $\sim 1\%$ at low Q, while the latter extends the measured Q range. A third detector array provides data at a high angle, $\phi=136°$. The energy resolution is shown in Fig. 3 as a function of the fractional energy transfer $\hbar\omega/E_i$. The signals from the detectors are sorted according to time of flight and scattering angle, and are normalized to a vanadium standard, so that the scattering cross section as a function of $\hbar\omega$ and Q can be derived.

The sample consisted of 80 g of sintered UO_2, in the form of six 7-mm-diam rods mounted in an aluminum can with 1-mm ^{10}B sheets placed between them in order to reduce multiple scattering. It was mounted onto the cold plate of a closed-cycle refrigerator giving temperatures down to 12 K, or in a standard RAL "orange" cryostat, giving a lower limit of 6.5 K. In order to reduce multiphonon scattering, all spectra were collected at temperatures lower than 50 K, with incident energies ranging from 228 to 1975 meV. Only transitions in which the neutrons lose energy can be observed at such a low temperature in UO_2 as the first-excited CF level is above 150 meV (1741 K).

III. EXPERIMENTAL RESULTS

The spectrum measured in the paramagnetic phase at $T=50$ K with an incident energy $E_i=290$ meV and a resolution (full width at half maximum) of 3.6 meV at $\hbar\omega=160$ meV is shown in Fig. 4. Two peaks are observed at 150 and 166 meV (1210 and 1339 cm^{-1}), in good agreement with the results of KLL. However, in the present measurements, it was possible to explore a much wider energy range, extending up to approximately 700 meV. A scan performed at $T=40$ K with an incident energy $E_i=1975$ meV and an energy resolution of 35 meV at $\hbar\omega=500$ meV shows that no more transitions of comparable intensity are visible above 200 meV (Fig. 5). Such a large incident energy was necessary to keep Q less than 5 $Å^{-1}$ for energy transfers of up to 600 meV.

The neutron spectra seen with an incident energy of 290 meV at four different temperatures between 6.5 and 35 K are shown in Fig. 6. Below the Néel temperature, there is more structure than could be resolved in the previous neutron measurements.[11] The two peaks seen above T_N are further split and the spectra may be fitted to four Gaussian line shapes. At $T=6.5$ K they are centered at 152.4, 162.2, 173.7, and 183.0 meV, respectively. The peak positions at different temperatures are summarized in Table I. It should be noted that the splitting of the upper peak is observed even above T_N, at $T=35$ K (Fig. 6). There is evidence, seen in Fig. 7, from scans made with $E_i=228$ meV and an energy resolution of 2.3 meV, that the lowest peak at 152.8 meV consists of two transitions split by about 2 meV. In Fig. 8 the theoretical form factor of U^{4+} ions is compared with the integrated

TABLE I. Temperature dependence of observed peak positions in meV.

Temperature (K)	Peak index 1	2	3	4
6.5	152.4±0.2	162.2±0.6	173.7±0.7	183.0±1.2
12	152.8±0.4	162.0±0.8	171.7±2.1	179.4±2.5
20	152.4±0.2	161.1±0.5	172.4±0.6	179.7±0.9
27	152.0±0.2	160.7±0.5	171.1±0.5	180.4±0.6
35	148.8±0.4	156.5±0.6	169.0±0.7	178.7±0.5

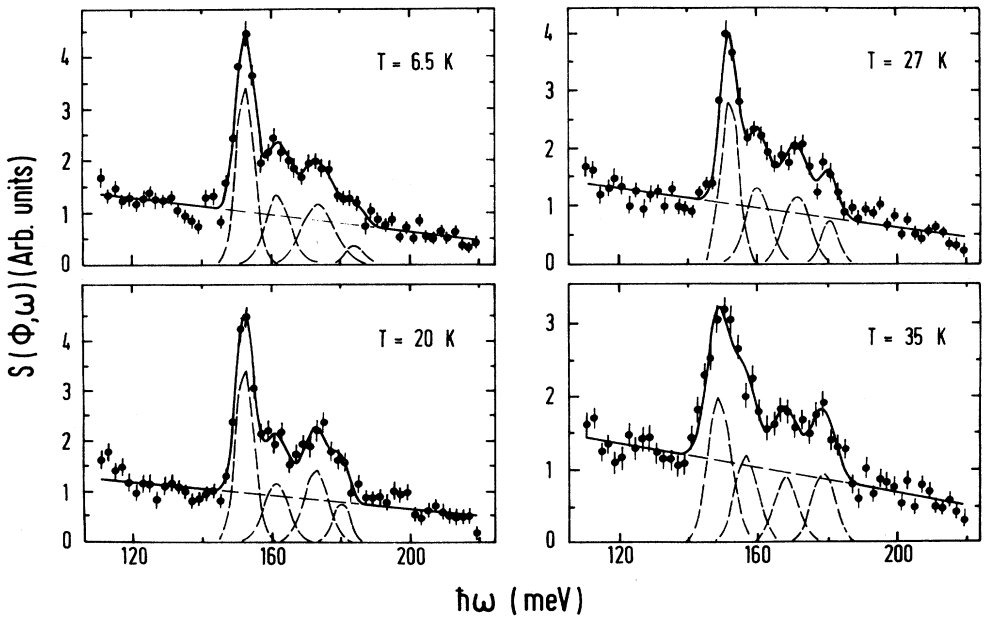

FIG. 6. Neutron spectra measured with $E_i = 290$ meV for different temperatures, between 6.5 and 35 K ($T_N = 30.8$ K). The smooth line is the fit to four Gaussian line shapes and a sloping background. These five components are shown by the dashed lines.

peak intensities measured at various scattering angles. The good agreement confirms the magnetic origin of the scattering. Moreover, the fact that the relative intensities of the different peaks does not change with Q tends to rule out the presence of a strong magnetovibrational component.

IV. ANALYSIS OF PARAMAGNETIC PHASE

The $5f^2$ configuration of the free U^{4+} ion consists of 13 multiplets, labeled $^{2S+1}L_J$ in the Russell-Saunders coupling scheme. Hund's rules give the $^3H_4$ multiplet as ground state. In the cubic crystalline environment of the paramagnetic phase of UO_2 (Fig. 9), the ninefold degeneracy of this lowest manifold is lifted by the CF potential into a Γ_1 singlet, a Γ_3 doublet, and two triplets, Γ_4 and Γ_5 (Fig. 10), where Γ_n labels the irreducible representation of the cubic point group. The molecular field and reduced crystalline symmetry of the antiferromagnetic phase lifts the residual degeneracy. The total Hamiltonian of the $5f^2$ configuration may be written as the sum of several terms in approximate order of strength

$$H = H_C + H_{s.o.} + H_{CF} + H_{QQ} + H_{ex} \ . \tag{3}$$

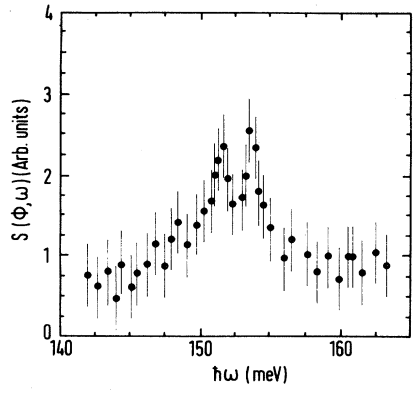

FIG. 7. High-resolution scan ($\Delta\hbar\omega = 2.3$ meV at 160 meV) showing the lowest peak at 152.8 meV split by about 2 meV at 12 K.

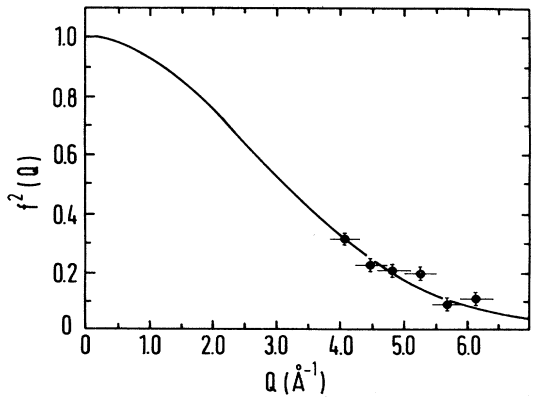

FIG. 8. Q dependence of the inelastic magnetic scattering intensity at 6.5 K, integrated between 140 and 190 meV and normalized to the value at 4 Å^{-1}. The solid line represents the square of the theoretical UO_2 magnetic form factor.

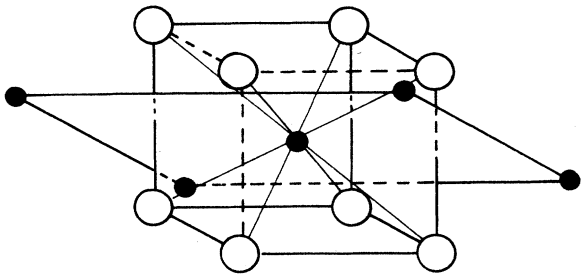

FIG. 9. Crystallographic environment of the U^{4+} ions (solid circles) in the paramagnetic phase of UO_2. The oxygen ions are represented by open circles.

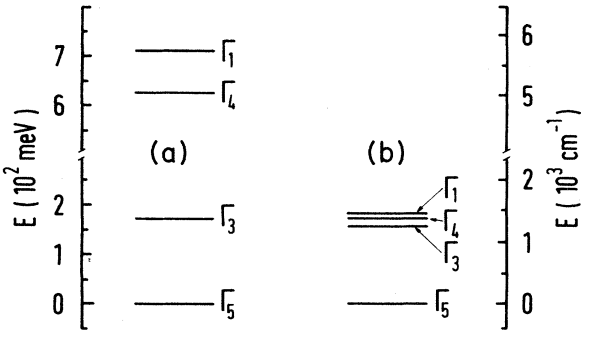

FIG. 10. Crystal-field energy-level scheme in the UO_2 paramagnetic phase as obtained (a) by Rahman and Runciman (Ref. 10), and (b) in the current experiment.

Here, H_C is the Coulomb interaction between the two $5f$ electrons, parametrized by the three Slater integrals F^2, F^4, and F^6, and $H_{s.o.}$ is the spin-orbit interaction, characterized by the coupling constant $\zeta_{s.o.}$. We have used the values of these parameters adopted by RR (see Table II). More recent estimates[17] require the inclusion of extra terms in the Hamiltonian representing configuration-interaction effects. However, as these only become important at energies higher than those under consideration here, they have been neglected in the present analysis. H_{CF} contains the cubic terms in the CF potential and H_{QQ} the additional CF contributions due to the lattice distortion, while H_{ex} is the exchange Hamiltonian. Well above T_N, the Hamiltonian consists of only the first three terms in Eq. (3) and may be diagonalized using the matrix elements calculated by Satten and Margolis[18] in the basis of $|LSJ\Gamma_n\rangle$ states.

The cubic CF Hamiltonian, in the RS or IC schemes, is given by[19]

$$H_{CF}=V_4\beta[\hat{O}_4^0(J)+5\hat{O}_4^4(J)] + V_6\gamma[\hat{O}_6^0(J)-21\hat{O}_6^4(J)] , \quad (4)$$

where $\hat{O}_n^m$ are the Stevens operator equivalents, β and γ are reduced matrix elements for the J manifold, and the parameters V_n are the coefficients of the CF potential; $V_n=A_n\langle r^n\rangle$, where $\langle r^n\rangle$ are the moments of the radial wave functions. H_{CF} can also be written in terms of the parameters x and W of Lea, Leask, and Wolf[20] as

$$H=W\left[\frac{x}{F(4)}[\hat{O}_4^0(J)+5\hat{O}_4^4(J)] + \frac{1-|x|}{F(6)}[\hat{O}_6^0(J)-21\hat{O}_6^4(J)]\right] . \quad (5)$$

The diagonalization of the complete Hamiltonian for the paramagnetic phase of UO_2, taking into account J mixing by the CF, was first carried out by RR, who proposed the Γ_5 triplet as a ground state, in agreement with a large number of experimental results.[1,2] The Γ_3 doublet is then the first-excited state followed by the Γ_4 triplet and the Γ_1 singlet (Fig. 10). In the absence of any direct experimental observations of the CF levels, RR adopted two constraints in determining V_4 and V_6. The first was that the ratio of V_6 to V_4 should be set to -0.06 given by the PCM. The second was that the reduction of the ordered moment in the antiferromagnetic phase, from $\mu_0=2.06\mu_B$ for the Γ_5 state in the IC approximation to the measured value of $\mu_0=1.74(2)\mu_B$,[3] could be attributed to J-mixing effects alone. In retrospect, neither of these assumptions is reliable, as will be discussed below. The quoted value of V_6/V_4 was obtained from the expression[10]

$$\frac{V_6}{V_4}=\frac{1}{21}\frac{\beta}{\gamma}\frac{1-|x|}{x} . \quad (6)$$

RR used the RS values for β and γ and fixed x to 0.9, the estimated value for Pr^{3+} ions in CaF_2. This is very close to the value of 0.89 given by the nearest-neighbor PCM using the radial integrals $\langle r^4\rangle=5$ a.u. and $\langle r^6\rangle=24.4$ a.u. calculated by Lenander.[21] However, x may be reduced to 0.84 by using the more recent relativistic determinations of $\langle r^4\rangle$ and $\langle r^6\rangle$, 7.632 and 47.774 a.u., respectively,[22] in a lattice-sum PCM in RS coupling.[23] This gives $V_6/V_4=-0.11$. Moreover, experience with rare-earth ionic systems shows that the PCM tends to underestimate the sixth-degree terms because of the neglect of overlap and covalency effects,[24] so a still lower value of x may be anticipated. This has been confirmed by two recent estimations. Scaling the available optical spectroscopy results for Np^{4+}:ThO_2 (Ref. 25) gives $x=0.82$,[23]

TABLE II. The cubic fourth- and sixth-degree crystal-field parameters using (1) current experimental results, (2) analysis of Rahman and Runciman (Ref. 10), (3) PCM calculations, and (4) a scaling procedure (Ref. 23). In 1, a J-mixing calculation has been used to fit the data taken at 50 K using the Slater integral parameters $F_2=23.73$ meV, $F_4=4.19$ meV, and $F_6=0.49$ meV, and the spin-orbit parameter $\zeta_{s.o.}=222.7$ meV.

	(1)	(2)	(3)	(4)
V_4 (meV)	−123.0	−409.0	−80.9	−50.0
V_6 (meV)	26.5	24.8	8.7	6.6
V_6/V_4	−0.22	−0.06	−0.11	−0.13

while recent *ab initio* calculations give $x=0.74$.[5]

RR showed that a reduced CF ground-state magnetic moment of $1.8\mu_B$ is obtained from J mixing if the following expression is satisfied,

$$V_4=-2250-5V_6\ , \tag{7}$$

where V_4 and V_6 are in cm^{-1}. It can be seen from Eq. (6) that the values of these parameters become unreasonably large as x decreases from 0.9 to 0.8. It has subsequently been shown by Allen[26] that the moment reduction can also arise through the strong magnetoelastic coupling evident in the spin-wave spectra of UO_2, and represented by the last two terms in the total Hamiltonian [Eq. (3)]. This point will be discussed in more detail in Secs. V and VI.

A further problem with the RR values of V_4 and V_6, -409 meV (-3300 cm^{-1}) and 24.8 meV (200 cm^{-1}), respectively (Table II), is that the CF transition energies given by them are not consistent with the neutron spectroscopy results. The $\Gamma_5\rightarrow\Gamma_3$ and $\Gamma_5\rightarrow\Gamma_4$ transitions are predicted to be at 169 and 624 meV, respectively. These should have comparable cross sections, but, as can be seen in Fig. 5, no peaks of the required size are visible up to 700 meV. The smooth line in Fig. 5 gives the estimated height of the $\Gamma_5\rightarrow\Gamma_4$ peak, assuming the resolution-limited peak at 160 meV arises entirely from the $\Gamma_5\rightarrow\Gamma_3$ transition, and corrected for the Q variation with energy. This should, in fact, be a lower estimate of the $\Gamma_5\rightarrow\Gamma_4$ peak height since the instrumental resolution improves with energy transfer.

A more satisfactory explanation of the current data is that both the $\Gamma_5\rightarrow\Gamma_3$ and $\Gamma_5\rightarrow\Gamma_4$ transitions are in the range 150–180 meV. (Note: the $\Gamma_5\rightarrow\Gamma_1$ transition is not a neutron dipole-allowed transition and so will be extremely weak.) It was pointed out by RR that the CF splittings were extremely sensitive to the ratio of V_6 to V_4 [see, e.g., Fig. 5 of KLL (Ref. 11)]. If we attribute the neutron groups observed at 150 and 166 meV to the $\Gamma_5\rightarrow\Gamma_3$ and $\Gamma_5\rightarrow\Gamma_4$ CF transitions, respectively, excellent agreement can be obtained with $V_4=-123$ meV and $V_6=26.5$ meV (Table III). The values of V_4 and V_6/V_4 are much closer to more recent estimates[23] than the RR values (see Table II). The energy-level scheme deduced from the two sets of parameters are shown in Fig. 10. The corresponding eigenstates are given in Table III. It can be seen that J-mixing effects are far less important than assumed by RR and cannot be responsible for the observed moment reduction. In particular, the Γ_5 ground state is practically a pure intermediate-coupling state.

TABLE III. The lowest eigenvalues and the three largest components of their eigenfunctions of the complete Hamiltonian (Coulomb, spin-orbit, and cubic crystal field) of UO_2 for two different values of the crystal field potential: (1) $V_4=-123$ meV and $V_6=26.5$ meV (present work), and (2) $V_4=-409$ meV and $V_6=24.8$ meV [Rahman and Runciman (Ref. 10)].

	J-mixing eigenfunctions	Energy (meV)
	(1) Present work	
Γ_5	$0.945\,^3H_4-0.308\,^1G_4+0.091\,^3F_4$	0.0
Γ_3	$0.835\,^3H_4-0.355\,^1G_4-0.353\,^3F_2$	150.1
Γ_4	$0.901\,^3H_4-0.284\,^1G_4-0.203\,^3F_3$	166.7
Γ_1	$0.965\,^3H_4-0.204\,^1G_4+0.096\,^3P_0$	174.8
	(2) Rahman and Runciman	
Γ_5	$0.874\,^3H_4-0.331\,^1G_4-0.214\,^3F_2$	0.0
Γ_3	$0.684\,^3H_4-0.530\,^3F_2+0.412\,^3H_5$	169.8
Γ_4	$0.781\,^3H_4-0.545\,^3H_{5b}-0.178\,^1G_4$	624.1
Γ_1	$0.749\,^3H_4+0.353\,^3P_0+0.342\,^3H_6$	710.0

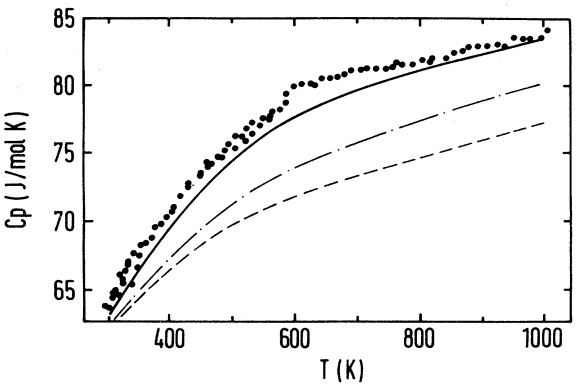

FIG. 11. Comparison between the specific heat of ThO_2 (dashed line) and UO_2 (dots). The dashed-dotted line is obtained by adding to the specific heat of ThO_2 the contributions arising from the thermal population of the magnetic energy levels of the U^{4+} ions, with the positions predicted by Rahman and Runciman (Ref. 10). The solid line is obtained if the currently proposed energy-level scheme is adopted.

Experimental support of the new CF level scheme is provided by two sources. First, the measured specific heat C_p of UO_2 has a Schottky contribution below 1000 K.[27] It may be assumed that the difference between the specific heat of UO_2 and ThO_2 arises entirely from the CF contribution, which is reasonable in the temperature range 300–1000 K given the similarity in their respective phonon dispersion relations.[28,29] Figure 11 shows the result of adding the calculated CF contribution to the measured specific heat of ThO_2 (Ref. 7) using the RR parameters (dashed-dotted line) and the present parameters (solid line). It is clear that the RR calculation significantly underestimates C_p, whereas the new parameters model the experimental measurements reasonably well. Agreement can be improved by adjusting the phonon contribution for the small difference in Einstein temperatures of the two compounds.[7] Second, infrared-absorption measurements show a strong feature at 515 meV,[2] which is close to the value of 520 meV predicted by the new parameters for the next Γ_5 level, which is predominantly of $^3F_2$ character. There is reasonable agreement with the positions of other peaks in the absorption spectrum, but since our calculations do not include configuration-interaction terms[17] they are of less value at higher energies.

V. ANALYSIS OF THE ANTIFERROMAGNETIC PHASE

A. Double-k model

The complex spectra observed in the ordered phase must be explained in terms of the combined effects of the

distorted CF potential and the molecular field (MF). We first consider the monoclinic internal distortion of the oxygen sublattice represented in Fig. 12. This was proposed by Faber and Lander,[3] who determined the oxygen displacement to be $\Delta_{\text{double-k}}=0.014$ Å. Calculations of the splittings of the cubic CF levels have been performed in the IC approximation with a molecular field parallel to [110]. In the following, the z axis is taken along the [001] direction and the x axis along the [110] direction, which is a principal axis of the susceptibility tensor.

For C_{2h} point symmetry, the CF Hamiltonian can be written in the form

$$H_{\text{CF}}=H_{\text{cubic}}+H_{\text{dist}} , \tag{8}$$

$$H_{\text{cubic}}=B_4(\hat{O}_4^0-5\hat{O}_4^4)+B_6(\hat{O}_6^0+21\hat{O}_6^4) , \tag{9}$$

with $B_4=V_4\beta$ and $B_6=V_6\gamma$,

$$H_{\text{dist}}=B_2^2\hat{O}_2^2+B_4^2\hat{O}_4^2+B_6^2\hat{O}_6^2+B_6^6\hat{O}_6^6 . \tag{10}$$

The omission of the other symmetry-allowed terms in Eq. (8) causes an error in the energy levels' position of less than 1%. Because of an axial rotation of the coordinate axes, the off-diagonal components of H_{cubic} have opposite signs to those in Eq. (4). The eigenstates of H_{cubic} are, for the $|\Gamma_1\rangle$ singlet,

$$|\Gamma_1^4\rangle=\epsilon(|4\rangle+|\bar{4}\rangle)-\gamma|0\rangle , \tag{11a}$$

for the $|\Gamma_3\rangle$ doublet,

$$|\Gamma_3^4\rangle=\frac{\gamma}{\sqrt{2}}(|4\rangle+|\bar{4}\rangle)+\sqrt{2}\epsilon|0\rangle , \tag{11b}$$

$$|\Gamma_3^2\rangle=\frac{1}{\sqrt{2}}(|2\rangle-|\bar{2}\rangle) , \tag{11c}$$

for the $|\Gamma_4\rangle$ triplet,

$$|\Gamma_4^{\pm3}\rangle=-\beta|\pm3\rangle-\alpha|\mp1\rangle , \tag{11d}$$

$$|\Gamma_4^4\rangle=\frac{1}{\sqrt{2}}(|4\rangle-|\bar{4}\rangle) , \tag{11e}$$

and for the $|\Gamma_5\rangle$ triplet,

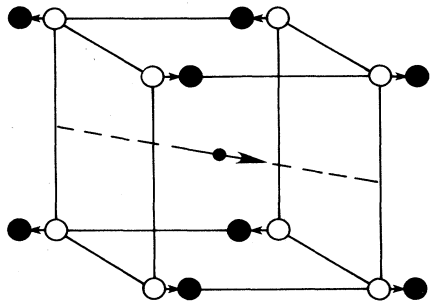

FIG. 12. Monoclinic internal distortion of the oxygen sublattice. The associated magnetic structure is double-**k** with the uranium magnetic moments (large arrow) pointing along the ⟨110⟩ directions. The oxygen displacement is $\Delta=0.014$ Å.

$$|\Gamma_5^{\pm3}\rangle=\alpha|\pm3\rangle-\beta|\mp1\rangle , \tag{11f}$$

$$|\Gamma_5^2\rangle=\frac{1}{\sqrt{2}}(|2\rangle+|\bar{2}\rangle) , \tag{11g}$$

where $\epsilon=0.456$, $\gamma=0.764$, $\alpha=0.935$, and $\beta=-0.354$. The corresponding eigenvalues E_n^c ($n=1,3,4,5$) are given as a function of the cubic CF parameters x and W by Lea, Leask, and Wolf.[20]

The eigenstates and eigenvalues in the presence of the distortion can be obtained by diagonalization of H_{CF} [Eq. (8)], using the cubic states as a basis. We define distortion matrix elements A, C, D, and G as linear combinations of the reduced CF parameters $b_2^m=B_2^m$, $b_4^m=60B_4^m$, and $b_6^m=1260B_6^m$,

$$A=\tfrac{1}{4}(7b_6^6+26b_2^2+2b_4^2-5b_6^2) , \tag{12a}$$

$$C=\tfrac{1}{4}(b_6^6+14b_2^2-14b_4^2+13b_6^2) , \tag{12b}$$

$$D=\frac{1}{\sqrt{3}}(2b_6^6+22b_2^2+2.5b_4^2+2b_6^2) , \tag{12c}$$

$$G=\frac{1}{\sqrt{7}}(-4b_6^6+14b_2^2+10.5b_4^2+4b_6^2) , \tag{12d}$$

and neglect terms which perturb the energy levels by less than 1%. The eigenstates and eigenvalues are given by

$$|\Gamma_5^{\pm}\rangle=\frac{1}{\sqrt{2}}(|\Gamma_5^3\rangle\pm|\Gamma_5^{-3}\rangle),\quad E_5^{\pm}=E_5^c\pm A ; \tag{13a}$$

$$|\Gamma_4^{\pm}\rangle=\frac{1}{\sqrt{2}}(|\Gamma_4^3\rangle\pm|\Gamma_4^{-3}\rangle),\quad E_4^{\pm}=E_4^c\pm C ; \tag{13b}$$

$$|\Gamma_{53}^{+}\rangle=\cos\theta|\Gamma_5^2\rangle+\sin\theta|\Gamma_3^4\rangle,\quad E_{53}^{+}=E_5^c\frac{1+\cos2\theta}{2}+E_3^c\frac{1-\cos2\theta}{2}+D\sin2\theta ; \tag{13c}$$

$$|\Gamma_{53}^{-}\rangle=-\sin\theta|\Gamma_5^2\rangle+\cos\theta|\Gamma_3^4\rangle,\quad E_{53}^{-}=E_5^c\frac{1-\cos2\theta}{2}+E_3^c\frac{1+\cos2\theta}{2}-D\sin2\theta ; \tag{13d}$$

$$|\Gamma_1^4\rangle,\quad E_1^4=E_1^c ; \tag{13e}$$

$$|\Gamma_{43}^{+}\rangle=\cos\phi|\Gamma_3^2\rangle+\sin\phi|\Gamma_4^4\rangle,\quad E_{43}^{+}=E_3^c\frac{1+\cos2\phi}{2}+E_4^c\frac{1-\cos2\phi}{2}+G\sin2\phi ; \tag{13f}$$

$$|\Gamma_{43}^{-}\rangle=-\sin\phi|\Gamma_3^2\rangle+\cos\phi|\Gamma_4^4\rangle,\quad E_{43}^{-}=E_3^c\frac{1-\cos2\phi}{2}+E_4^c\frac{1+\cos2\phi}{2}-G\sin2\phi ; \tag{13g}$$

where

$$\tan 2\theta = \frac{2D}{E_5^c - E_3^c} , \tag{14}$$

$$\tan 2\phi = \frac{2G}{E_3^c - E_4^c} . \tag{15}$$

Values of the energy levels and eigenfunction coefficients calculated for four models of this distortion, together with the corresponding x, W, and b_n^m values, are given in Table IV. These models are the nearest-neighbor (NN) and lattice-sum (LS) point-charge models in both the RS and IC schemes. The IC to RS ratios $\alpha=0.924$, $\beta=0.993$, and $\gamma=0.889$ have been used for the Stevens factors.[30] The relative position of the energy levels, with respect to the corresponding cubic levels, is shown in Fig. 13 for the case of the IC-NN model.

The effects of the molecular field (MF) must now be considered. We assume that the direction of the field is [110], i.e., the x axis. This simplifies the calculation by reducing the size of the matrices that need to be diagonalized. First of all, we consider the effect of the MF within the ground Γ_5 triplet. The aim is to find the self-consistency condition which gives the value (or at least the order of magnitude) of the MF which can account for both the ordered moment at $T=0$ K ($\mu_0=1.74\mu_B$) and the ordering temperature $T_N=30.8$ K. The Hamiltonian is now

$$H = H_{\rm CF} + H_{\rm MF} , \tag{16}$$

TABLE IV. Eigenvalues and coefficients of the eigenfunctions for the crystal-field Hamiltonian calculated with different approximations assuming a monoclinic distortion of the oxygen sublattice. RS, Russell-Saunders coupling; IC, intermediate-coupling approximation. The energy unit is meV (1 meV = 8.065 cm^{-1}). The Lea, Leask, and Wolf parameters x and W and the b_n^m's in the various cases are also given.

	Nearest neighbors		Lattice sum	
	RS	IC	RS	IC
E_5^+	0.0	0.0	0.0	0.0
E_{53}^+	4.0	3.7	4.6	4.3
E_5^-	9.0	8.4	10.9	10.2
E_{43}^+	170.0	164.5	159.3	154.6
E_{53}^-	175.6	168.5	169.7	162.2
E_4^+	177.0	173.8	163.2	160.6
E_4^-	178.4	175.1	165.6	162.0
E_1^4	181.2	183.6	158.1	160.6
E_{43}^-	182.8	177.9	177.9	167.9
$\sin\theta$	0.0564	0.0564	0.0699	0.0678
$\cos\theta$	0.9984	0.9985	0.9976	0.9977
$\sin\phi$	0.6303	0.5094	0.8079	0.7170
$\cos\phi$	0.7763	0.8605	0.5894	0.6970
x	0.86	0.88	0.84	0.86
W (meV)	4.6	4.5	4.2	4.1
b_2^2	−0.694	−0.641	−0.838	−0.775
b_4^2	−0.566	−0.562	−0.565	−0.562
b_6^2	−0.108	−0.096	−0.108	−0.096
b_6^6	0.079	0.070	0.078	0.069

with

$$H_{\rm MF} = -\boldsymbol{\mu}\cdot\mathbf{H}_m = -hJ_x \tag{17}$$

and

$$h = g_J\mu_B H_m . \tag{18}$$

The diagonalization of the corresponding energy matrix for the ground triplet leads to the ground state

$$|\Gamma^{(0)}\rangle = \cos\eta|\Gamma_5^+\rangle + \sin\eta|\Gamma_{53}^+\rangle , \tag{19}$$

with energy

$$E^{(0)} = E_5^+\frac{1+\cos 2\eta}{2} + E_{53}^+\frac{1-\cos 2\eta}{2} - hf(\theta)\sin 2\eta . \tag{20}$$

The next-excited states are

$$|\Gamma^{(a)}\rangle = |\Gamma_5^-\rangle \tag{21}$$

and

$$|\Gamma^{(b)}\rangle = -\sin\eta|\Gamma_5^+\rangle + \cos\eta|\Gamma_{53}^+\rangle , \tag{22}$$

with energies

$$E^{(a)} = E_5^- , \tag{23}$$

$$E^{(b)} = E_5^+\frac{1-\cos 2\eta}{2} + E_{53}^+\frac{1+\cos 2\eta}{2} + hf(\theta)\sin 2\eta , \tag{24}$$

respectively. Here, the parameters η and $f(\theta)$ are defined by

$$\tan 2\eta = \frac{2hf(\theta)}{E_{53}^+ - E_5^+} , \tag{25}$$

$$f(\theta) = 2.5\cos\theta + \sqrt{3}\sin\theta . \tag{26}$$

As the mixing between the Γ_5 and Γ_3 states is small (see Table IV), $f(\theta)\simeq 2.5$. The effect of the MF on the excit-

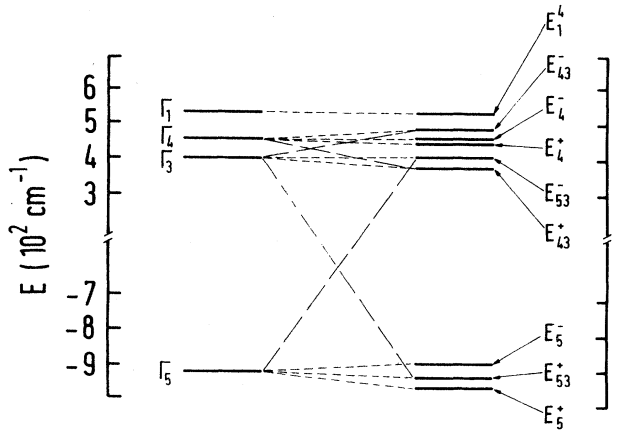

FIG. 13. Splitting of the cubic crystal-field levels due to a monoclinic distortion of the oxygen ligand cage.

ed states as a function of the parameter h can be determined numerically, once the cubic and distortion parts of H are fixed. The eigenstates have the form

$$|\Gamma^{(\mu)}\rangle = c_1^\mu|\Gamma_{43}^+\rangle + c_2^\mu|\Gamma_{43}^-\rangle + c_3^\mu|\Gamma_4^-\rangle \quad (\mu=1,4,5)\ ,$$
$$|\Gamma^{(\mu)}\rangle = c_1^\mu|\Gamma_{53}^-\rangle + c_2^\mu|\Gamma_1^4\rangle + c_3^\mu|\Gamma_4^+\rangle \quad (\mu=2,3,6)\ . \tag{27}$$

The ordered magnetic moment at $T=0$ K lies along the x axis and is given by

$$\mu_0 = \langle\mu_x\rangle_0 = g_J \sin(2\eta) f(\theta)\ . \tag{28}$$

Although in the present CF model for UO_2 the molecular field approach cannot be consistent with the evidence of a first-order transition at T_N, we can at least estimate the value of H_m. By assuming $H_m=\lambda M$, where $M=N_A\mu_B\langle\mu_x\rangle_0$ is the magnetization in molar units and N_A is Avogadro's number, and comparing with Eq. (18), one obtains

$$\langle\mu_x\rangle_0 = \frac{3.836h}{g_J\lambda}\ , \tag{29}$$

with $\langle\mu_x\rangle_0$ in Bohr magnetons and the molecular field constant λ in molar units. In the MF approximation, λ is given by the reciprocal of the molar Van Vleck susceptibility along the easy [110] axis, calculated at T_N using the CF alone, i.e., setting the molecular field to zero. It can be shown that in a three-level model, which is appropriate in the present case since only the ground triplet is involved in the transition, one has

$$\lambda^{-1} = 0.521 g_J^2 f^2(\theta)(1-e^{-\Delta/k_BT_N})/\Delta Z(T_N)\ , \tag{30}$$

with $\Delta=E_{53}^+-E_5^+$, and $Z(T)$ the partition function in the adopted three-level scheme. By substituting into Eq. (29) and comparing the result with Eq. (28), the following expressions are obtained:

$$h = \frac{\Delta}{2f(\theta)}\left[\frac{Z^2(T_N)}{(1-e^{-\Delta/k_BT})^2}-1\right]^{1/2}\ , \tag{31}$$

$$\langle\mu_x\rangle_0 = g_J f(\theta)\left[1-\frac{(1-e^{-\Delta/k_BT})^2}{Z^2(T_N)}\right]^{1/2}\ . \tag{32}$$

It should be noted that in the absence of distortion, $\langle\mu_x\rangle_0=2.5g_J$, which is the correct value for a degenerate Γ_5 triplet ($2.06\mu_B$ in the IC approximation). Using the quoted formulas we obtain, in the NN-IC case, $h=8$ cm^{-1} and $\langle\mu_x\rangle_0=1.73\mu_B$, in excellent agreement with the experimental value.

In order to discuss the neutron scattering results, the transition probabilities from the ground to the excited states must be calculated. Because the system is anisotropic, and the chosen axes are the principal ones for the magnetic moment and the susceptibility tensors, the magnetic dipole matrix elements occurring in the cross section for inelastic neutron scattering are given by

$$P_{n\to m} = \tfrac{2}{3}(|\langle n|J_x|m\rangle|^2 + |\langle n|J_y|m\rangle|^2 + |\langle n|J_z|m\rangle|^2)\ . \tag{33}$$

Considering only transitions from the ground state $|\Gamma^{(0)}\rangle$, the following expressions are obtained:

$$|\langle\Gamma^{(0)}|J_x|\Gamma^{(\mu)}\rangle|^2 = 0\ , \tag{34a}$$

$$|\langle\Gamma^{(0)}|J_y|\Gamma^{(\mu)}\rangle|^2 = \left[\left(\frac{\sqrt{7}}{2}\sin\phi-\cos\phi\right)q_1^\mu + \left(\sin\phi+\frac{\sqrt{7}}{2}\cos\phi\right)q_2^\mu + \left(\sqrt{7/3}\sin\theta-\frac{\sqrt{7}}{2}\cos\theta\right)p_3^\mu\right]^2\ , \tag{34b}$$

$$|\langle\Gamma^{(0)}|J_z|\Gamma^{(\mu)}\rangle|^2 = \left[2\left(\cos\theta\cos\phi+\sqrt{7/3}\sin\theta\sin\phi\right)p_1^\mu + 2\left(\sqrt{7/3}\sin\theta\cos\phi-\cos\theta\sin\phi\right)p_2^\mu + \sqrt{7/4}q_3^\mu\right]^2\ , \tag{34c}$$

for $\mu=1,4,5$, and

$$|\langle\Gamma^{(0)}|J_y|\Gamma^{(\mu)}\rangle|^2 = |\langle\Gamma^{(0)}|J_z|\Gamma^{(\mu)}\rangle|^2 = 0\ ,$$
$$|\langle\Gamma^{(0)}|J_x|\Gamma^{(\mu)}\rangle|^2 = \left[\left(\sqrt{3}\cos\theta-2.5\sin\theta\right)q_1^\mu - \left(\frac{\sqrt{7}}{2}\cos\theta+\sqrt{7/3}\sin\theta\right)p_3^\mu\right]^2 \tag{35}$$

for $\mu=2,3,6$ ($p_i^\mu=c_i^\mu\sin\eta$, $q_i^\mu=c_i^\mu\cos\eta$).

The position of the energy levels, relative to the ground energy, and the corresponding transition probability, are shown in Fig. 14 as a function of x, for $h=0$, 8, and 13 cm^{-1}. $h=13$ cm^{-1} has been chosen because it is the value which self-consistently gives the measured values of $T_N=30.8$ K and $\mu_0=2.1\mu_B$, in the absence of lattice distortion. It is also very close to the value used by Allen[26] to fit the spin-wave spectra ($h=8J/5\simeq 14$ cm^{-1}). The scaling parameter W is set to 35 cm^{-1}, the value giving the best fit to the CF levels in the paramagnetic phase. In all cases, the distortion parameters are those corresponding to the NN-IC model.

It is evident that the modification of the CF by the lattice distortion is the dominant factor in splitting the cubic CF levels. The molecular field mixes the CF states, and thus has a strong effect on the transition probabilities but little effect on their energies. Figure 14 shows that the observed level positions for $T>T_N$ can be accounted for, in this approximation, with x in the range of values reported in Table IV. However, the splitting of the Γ_3 doublet is too large, and that of the Γ_4 triplet too small, to account for the experimental spectra below T_N. It is not possible to improve the agreement either by varying h

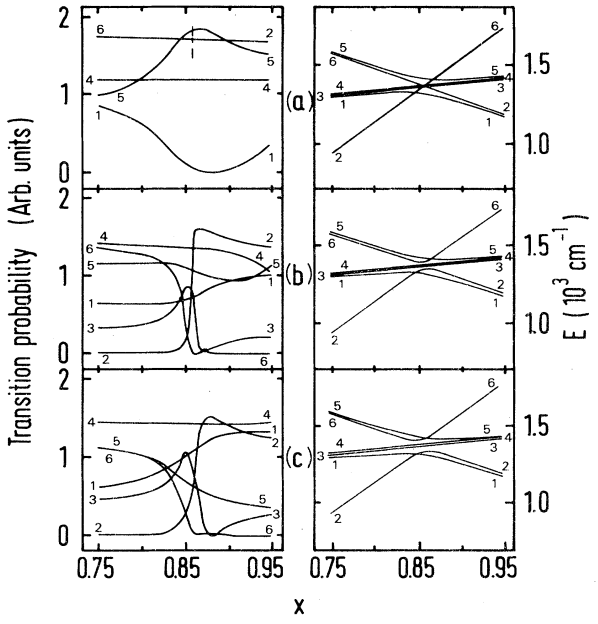

FIG. 14. Excited energy levels and corresponding transition probabilities (P) from the ground state as a function of the cubic crystal-field parameter x, for $W=35$ cm^{-1} and different values of the molecular field: (a) $h=0$, (b) $h=8$ cm^{-1}, and (c) $h=13$ cm^{-1}. A monoclinic distortion of the oxygen sublattice is assumed. In case (a), $P_3=P_6=0$ for $x>\frac{6}{7}$ and $P_3=P_2=0$ for $x<\frac{6}{7}$.

or b_2^2, the dominant term in H_{dist}. This is a consequence of the fact that, in the double-**k** model, the Γ_3 quadrupole moment is relatively large, while both the quadrupole and magnetic dipole moments of the Γ_4 triplet are intrinsically small. It seems unlikely that J-mixing effects will alter these conclusions significantly, because the Γ_3 and Γ_4 states are still predominantly $^3H_4$ (see Table III). It is therefore necessary to consider if the triple-**k** model can give more satisfactory results.

B. Triple-k model

The occurrence of a triple-**k** magnetic structure in UO_2 is suggested by the results of a neutron diffraction study[12] performed on a single crystal with a strong external magnetic field applied along [001]. The proposed structure preserves the cubic symmetry and is characterized by magnetic moments lying along $\langle 111\rangle$ directions. The distortion of the oxygen sublattice should then be considered as the superposition of three frozen transverse phonon modes having the components of the star of $(2\pi/a_0)\{1,0,0\}$ as wave vectors. The oxygen ions at the corners of the fluorite cube are shifted by a quantity $\Delta_{\text{triple-k}}=\Delta_{\text{double-k}}/\sqrt{3}$ along the $\langle 111\rangle$ directions defined by the magnetic moments of the neighboring uranium ions.[31] The two possible configurations, corresponding to pairs of oxygen ions moving (a) towards or (b) away from a U^{4+} ion, are shown in Fig. 15.

In a reference frame with the z axis parallel to the magnetic moment direction (the z' axis in Fig. 15), the CF

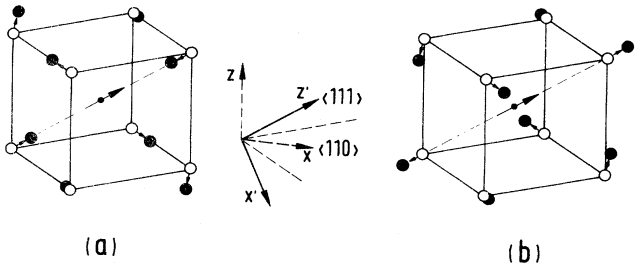

FIG. 15. Triple-**k** distortion of the oxygen sublattice. The uranium ion is represented by the small circle. The associated magnetic structure is triple-**k** with the uranium magnetic moments (large arrow) pointing towards $\langle 111\rangle$ directions. The oxygen ions are shifted (a) towards or (b) away from a U^{4+} ion, along the lines defined by the magnetic moment direction. The reference frame in which the crystal-field problem is analyzed is also shown.

Hamiltonian is given by

$$H_{\text{CF}}=B_2^0\hat{O}_2^0+B_4^0\hat{O}_4^0+B_4^3\hat{O}_4^3+B_6^0\hat{O}_6^0+B_6^3\hat{O}_6^3+B_6^6\hat{O}_6^6\,. \tag{36}$$

It can be shown that the fourth- and sixth-degree terms are not appreciably different from the cubic terms when written in the rotated reference frame adopted here. The main contribution to the distortion is then provided by the $B_2^0\hat{O}_2^0$ term. In the point-charge approximation, one obtains $B_2^0\simeq\pm 3$ cm^{-1}, taking the oxygen ion to have an effective charge $Z=2$, with the positive and negative signs holding in case (b) and (a) of Fig. 15, respectively. As a result, the two triplet Γ_5 and Γ_4 levels are both split into a doublet and a singlet, so that the cubic states are split into three doublets and three singlets as shown in Fig. 16. The ground state is a doublet in case (a) and a singlet in case (b). In the rotated reference frame, the cubic states are given as linear combinations of the $|J,J_z\rangle$ vectors, in which the J_z components differ by 3. The distortion term $B_2^0\hat{O}_2^0$ only changes the coefficients of these states. The same is true of the molecular field term, which in the rotated frame is given by

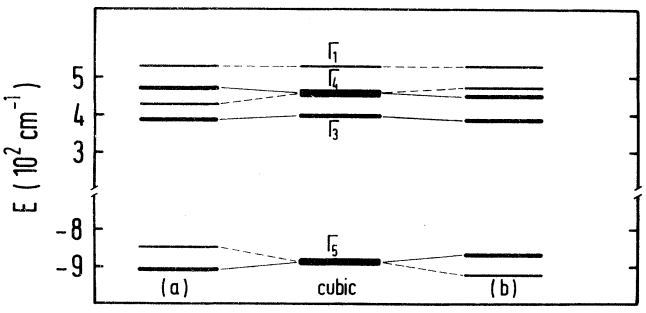

FIG. 16. Splitting of the cubic crystal field levels due to the triple-**k** distortions shown in Fig. 15. The ground state is (a) a doublet or (b) a singlet if the oxygens move towards or away from the U^{4+} ions, respectively ($W=35$ cm^{-1}, $x=0.88$).

$$H_{\mathrm{MF}} = -hJ_z \ . \tag{37}$$

The final states are of the type

$$\begin{aligned} |\Gamma_i^0\rangle &= a_1^{(i)}|3\rangle + a_2^{(i)}|0\rangle + a_3^{(i)}|\bar{3}\rangle \quad (i=1,4,5) \\ |\Gamma_j^{\pm}\rangle &= b_1^{(j)}|\pm 4\rangle + b_2^{(j)}|\pm 1\rangle + b_3^{(j)}|\mp 2\rangle \quad (j=3,4,5) \end{aligned} \tag{38}$$

The states $|\Gamma_j^{\pm}\rangle$ are degenerate doublets in the absence of a molecular field. Here the indices i and j refer to the unperturbed cubic manifolds. Since, in the present case, there is no particular advantage in solving the eigenvalue problem by using the cubic states as the basis set, the coefficients of the states Eq. (38) and their energy values are found by direct numerical diagonalization of the corresponding 3×3 blocks in the $|J,J_z\rangle$ basis. Following a procedure similar to that adopted for the double-**k** magnetic structure, the matrix elements for the magnetic dipole transitions can be calculated. The ground states in cases (a) and (b) are $|\Gamma_5^+\rangle$ and $|\Gamma_5^0\rangle$, respectively. The ordered moment of the magnetic $|\Gamma_5^+\rangle$ state is slightly higher than $2\mu_B$, i.e., the fully saturated moment of the $|+1\rangle$ state of an effective $S=1$ ground multiplet.[31] The enhancement is due to the interaction with the excited states, which are included in the present calculation. On the other hand, the $|\Gamma_5^0\rangle$ state is nonmagnetic. Therefore, the ordered moment in case (b) is zero at $T=0$ K, unless the molecular field h is strong enough to induce a crossover between the $|\Gamma_5^0\rangle$ and the $|\Gamma_5^+\rangle$ states. There is an abrupt change to $\mu_0 \simeq 2\mu_B$ when $h \geq 30$ cm^{-1}, but this value of h is unrealistically large, as will be clear in the following discussion. Moreover, with such a high value of h the calculated level spacings and transition probabilities are not consistent with the experimental observations.

A $|\Gamma_5^+\rangle$ ground state is consistent with the interpretation of the origin of the oxygen sublattice distortion as an effect of quadrupolar ordering. When the ground state of the uranium ion is magnetic, the electronic charge cloud in real space is flattened perpendicular to the spin direction, thus favoring a shorter U-O distance along the z' axis.[4,31] In other words, when the $|\Gamma_5^+\rangle$ state is the lowest, the expectation value of the quadrupole moment in the effective quadrupole-quadrupole Hamiltonian[31] changes its sign leading to a negative CF axial parameter B_2^0 as in case (a) of Fig. 15. In view of these arguments, only this kind of distortion will be considered in the following.

The CF transitions and their corresponding probabilities for the triple-**k** distortion with $B_2^0 = -3$ cm^{-1} are shown in Fig. 17 as a function of the cubic CF parameter x, for $W=35$ cm^{-1} and three values of the molecular field h, namely $h=0$ [Fig. 17(a)], $h=8$ cm^{-1} [Fig. 17(b)], and $h=13$ cm^{-1} [Fig. 17(c)]. These are the same values of h as quoted in the double-**k** case [Fig. 14] and are indicative of the likely magnitude of the exchange interaction. As discussed in Sec. V A, the value of $h=13$ cm^{-1} corresponds to the self-consistent solution of the CF-plus-MF problem in the undistorted cubic case, for $T_N=30.8$ K. In the presence of the triple-**k** distortion, the value of h decreases to about 8 cm^{-1}. However, a higher value of h, corresponding to a higher value of the

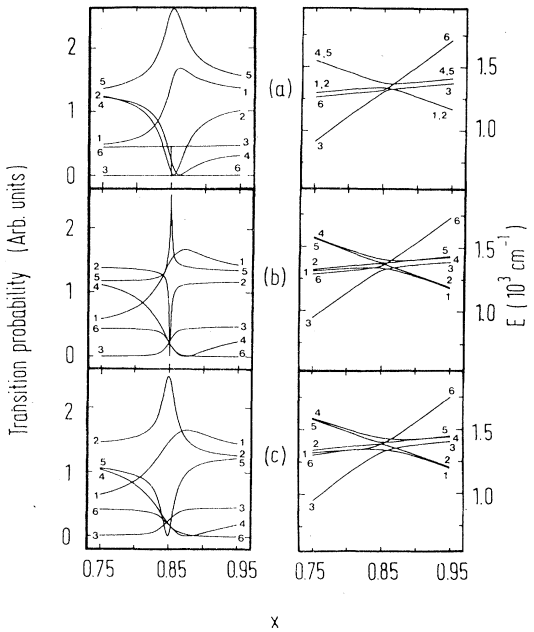

FIG. 17. Transition energies and probabilities as a function of the cubic crystal-field parameter x, for $W=35$ cm^{-1}, (a) $h=0$, (b) $h=8$ cm^{-1}, and (c) $h=13$ cm^{-1}. A triple-**k** distortion and magnetic structure are assumed, with oxygen moving towards the U^{4+} ions ($B_2^0 = -3$ cm^{-1}).

hypothetical second-order transition temperature, is more appropriate given the first-order character of the actual transition. A value of $h=13$ cm^{-1}, which gives $T_N=46$ K, should be considered an upper limit because, as will be discussed in the next section, larger values lead to unacceptably high values of T_N, even in theories that take account of the first-order character of the transition.[26,31] It should be pointed out, however, that the exchange integral splitting the excited cubic CF states could, in principle, be different from that splitting the ground triplet.

As can be seen in Fig. 17, the calculated level spacings are not significantly affected by the molecular field. The dominant contribution to the splitting comes from the lattice distortion. It is the transition probabilities which are sensitive to h, as in the double-**k** model.

VI. DISCUSSION

The different splittings calculated for the double-**k** and triple-**k** models in UO_2 are illustrated in Fig. 18, which shows the CF-level spacings and transition probabilities calculated in the IC approximation for the set of parameters which give the best fit to the experimental data ($B_2^0 = -3$ cm^{-1}, $W=33$ cm^{-1}, $x=0.90$, and $h=13$ cm^{-1}). The dashed lines represent the results of the measurements performed at $T=12$ K with an incident energy of 290 meV. They are normalized so that the first unresolved peak has an intensity equal to the sum of the two calculated $\Gamma_5 \rightarrow \Gamma_3$ transitions. The uppermost experimental level is close to the position calculated for the transition from the ground state to the highest singlet

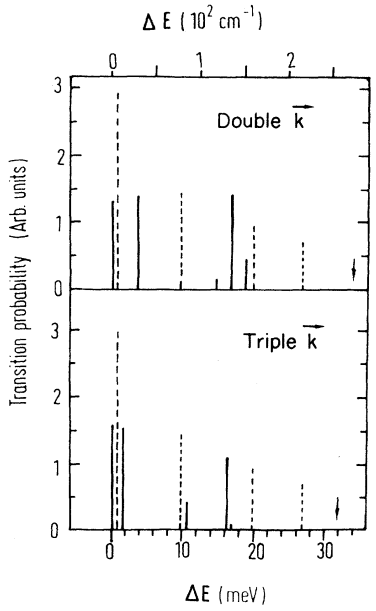

FIG. 18. Crystal-field-level spacing and transition probabilities calculated by the point-charge model (intermediate-coupling approximation) assuming either a double-**k** or a triple-**k** magnetic structure. The dashed lines represent the experimental observations taken at 12 K normalized as discussed in the text. The parameters used are $W=33$ cm^{-1}, $x=0.90$, and $h=13$ cm^{-1}. The arrows indicate the positions calculated for the transition to the highest singlet.

($\Delta E=34$ and 32 meV in the double-**k** and triple-**k** model, respectively). However, in the absence of J mixing, this transition has nearly zero cross section.

Whereas the neutron spectroscopy results are not consistent with the double-**k** model, the triple-**k** model accounts well for the main features of the experimental spectrum, as is seen clearly from Fig. 18. The splitting of the $\Gamma_5\rightarrow\Gamma_3$ transition remains very small under a triple-**k** distortion, in contrast to the double-**k** case, and is in agreement with the experimental observations (Fig. 7). Moreover, the triple-**k** model gives rise to a larger splitting of the $\Gamma_5\rightarrow\Gamma_4$ transitions, which accounts for the position of the next two peaks more satisfactorily. The agreement cannot be improved by varying h or B_2^0.

The value of B_2^0 used in Fig. 18 is the PCM estimation of about -3 cm^{-1}, obtained with an effective charge $Z=2$ on the oxygen ions and a distortion amplitude fixed at the experimental value.[3] We can compare our parameters with those used in the mean-field treatment of the magnetoelastic and exchange interaction by Giannozzi and Erdös.[31,32] In their work, the ground state was treated as an isolated effective spin $S=1$ (corresponding to the Γ_5 state) with the Hamiltonian

$$H=-J\langle S\rangle S+3K\langle Q\rangle Q\ , \tag{39}$$

where $\langle Q\rangle$ and $\langle S\rangle$ are the expectation values of the quadrupole moment and effective spin operators, respectively, K is a negative constant proportional to the square of the oxygen ions' effective charge, and J is the positive exchange integral determining the transition temperature in the type I antiferromagnetic structure with anisotropic exchange.

It can be shown that the following correspondences hold:

$$6.5B_2^0\leftrightarrow K\langle Q\rangle,\quad 2.5h\leftrightarrow J\langle S\rangle\ . \tag{40}$$

In Refs. 31 and 32, Z was determined by the self-consistency condition on the distortion parameter $\Delta_{\text{triple-k}}$ to be $Z=0.95$, leading to the value $K=31$ cm^{-1} when the value of $\langle r^2\rangle$ given in Ref. 22 is used. Since $\langle Q\rangle=\frac{1}{3}$ when the lowest state is the $|+1\rangle$ component of the ground triplet, we obtain $B_2^0=-1.6$ cm^{-1} from Eq. (40). Therefore, the quoted value of Z is too small to account for the high-energy neutron spectra, which need twice this value, i.e., $Z\simeq 2$ in the present approach. Furthermore, a lower Z could not account for the size of the cubic CF parameters V_4 and V_6 measured in the paramagnetic phase (Table II). The parameter Z used by Giannozzi and Erdös[31] is, in fact, a "dynamically effective" anionic charge.[33] While this PCM parameter may explain the magnetoelastic origin of the distortion, it cannot be used to determine the overall CF-level scheme.

Another important experimental observation is the first order of the phase transition at T_N.[3] It can be shown, following the approach of Chen and Levy,[34] that the effective Hamiltonian [Eq. (39)] leads to a first-order transition to a spin-ordered structure at $T_N>5h/3k_B$ if $1<5h/(39|B_2^0|)<2$ ($k_B=0.695$ cm^{-1}/K is Boltzmann's constant). With $T_N=31$ K, $h=13$ cm^{-1} is an upper limit for the molecular field parameter, so that $|B_2^0|$ needs to be smaller than 1.67 cm^{-1} in order to have a first-order magnetic transition at $T_N\leq 31$ K. In our opinion, this discrepancy in the value of $|B_2^0|$ is not a serious problem, given the simplifications in the effective Hamiltonian [Eq. (39)] and in the approximation we have used. On the contrary, the constraint on the value of h provided by T_N ensures that the observed splitting of the cubic CF levels arises mainly from the lattice distortion, as indicated in Fig. 17.

Similar conclusions can be drawn concerning the order of magnitude of the B_2^2 parameter if the double-**k** model is used. A first-order magnetic transition at T_N would require a value of $|B_2^2|$ lower than the calculated one (~ 6 cm^{-1}) by nearly a factor 2, with the molecular field parameter $h\simeq 10$ cm^{-1} and $\mu_0=1.9\mu_B$. This can be seen from comparisons of the work of Chen and Levy,[34] with Eq. (16) when only the leading $B_2^2\hat{O}_2^2$ distortion term is taken into account. Thus, both the double-**k** and triple-**k** models have difficulties in explaining the first-order character of the phase transition.

The neutron spectra taken at $T=35$ K just above T_N show that the splitting of the cubic CF levels is still present in the paramagnetic phase. This is probably a result of the dynamic Jahn-Teller effect, discussed by Sasaki and Obata,[35] evidence of which persists to at least 200 K.[36] The observation that the magnitude of the splittings hardly changes through T_N, even though the molecular field falls to zero, is consistent with our conclusion that the CF energies are hardly affected by the value of h.

However, we would expect the transition probabilities to be quite different above and below T_N, and, indeed, Fig. 6 shows that there is a considerable change in the intensity distribution for $T > T_N$.

Returning to the cubic CF, the value of V_4 can be interpreted in terms of the Newman superposition model[24] to give an intrinsic two-ion CF parameter $\overline{A}_4 = 39.5$ meV. This brings UO_2 in line with the other tetravalent uranium compounds discussed by Newman,[37] Cs_2UCl_6, Cs_2UBr_3, and zircon, whereas the RR value is anomalously large ($\overline{A}_4 = 131$ meV). The PCM with an effective charge $Z = 2$ on the oxygen ions gives a reasonable estimate of the CF parameters and therefore of the whole CF splitting. This result is also consistent with recent neutron inelastic scattering experiments on UOS. In this isoelectronic compound,[38] the overall splitting and structure of the CF levels are also in agreement with the prediction of PCM calculations, originally used to account for the Schottky contributions to the specific heat and the ordered moments in the uranium oxychalcogenides.[39]

Finally, the paramagnetic susceptibility, which is reported to follow a Curie-Weiss law in the range 77–1100 K,[40] with $\mu_{\text{eff}} = 3.2\mu_B$ and $\Theta_P = -220$ K, cannot be interpreted in terms of the CF splitting of the ground multiplet alone. The calculated μ_{eff} approaches the asymptotic IC value of $2.68\mu_B$ too rapidly, while the paramagnetic temperature is about twice that inferred from estimates of the exchange integrals and critical scattering.[32] This discrepancy, which is not unusual in uranium compounds, should be the object of further analysis.

VII. CONCLUSIONS

Neutron spectroscopy results have shown that the CF potential previously proposed by RR is too strong and that the ground state is, to a good approximation, a pure intermediate-coupling state, with only slight modification by J-mixing effects. The new values of the cubic CF parameters are $V_4 = -123$ meV and $V_6 = 26.5$ meV. The observed energy levels are consistent with the high-temperature specific-heat data and infrared absorption. In the antiferromagnetic phase below $T_N = 30.8$ K, the observed splittings of the CF levels have been interpreted in terms of the combined effects of the molecular field and the distortion of the oxygen ligand cage surrounding the U^{4+} ions. Both the double-**k** and triple-**k** models have been considered. The calculated energy spacings indicate a triple-**k** distortion and demonstrate that inelastic neutron scattering may be used to provide structural information when neutron diffraction cannot give an unambiguous answer.

In spite of the advance in our understanding of UO_2 provided by these measurements, there are many unsolved problems. First of all, the reduced value of the ordered moment cannot be explained in the triple-**k** structure without invoking a new mechanism. The double-**k** model would produce a moment reduction in a simple molecular field approach, but cannot account for the order of the transition. Allen's theory,[26] which does account for both the reduced moment and the first-order character of the transition, does not employ the experimentally observed distortion.[3] The theoretical stability of the various proposed structure is also problematic; although the triple-**k** structure is calculated to be more stable than the double-**k** structure, it is less stable than Allen's single-**k** structure.[31]

ACKNOWLEDGMENTS

This work was supported in part by the Science and Engineering Research Council (SERC), United Kingdom, the United Kingdom Atomic Energy Authority (UKAEA) General Nuclear Safety Programme, and the Underlying Research Programme of the UKAEA. We are extremely grateful to Dr. M. A. Mignanelli for the preparation of the sample used.

*Present address: Dipartimento di Scienze dei Materiali e della Terra, Università degli Studi di Ancona, I-60131 Ancona, Italy.

[1]J. M. Fournier, Struct. Bonding (Berlin) **59/60**, 127 (1985).
[2]J. Schoenes, Phys. Rep. **63**, 301 (1980).
[3]J. Faber, Jr. and G. H. Lander, Phys. Rev. B **14**, 1151 (1976); **13**, 1177 (1976); B. C. Frazer, G. Shirane, D. E. Cox, and C. E. Olsen, Phys. Rev. **140**, 1448 (1965).
[4]W. J. L. Buyers and T. M. Holden, in *Handbook on the Physics and Chemistry of the Actinides,* edited by A. J. Freeman and G. H. Lander (Elsevier, Amsterdam, 1985).
[5]Z. Gajek, M. P. Lahalle, J. C. Krupa, and J. Mulak, J. Less-Common Met. **139**, 351 (1988).
[6]P. Browning, G. J. Hyland, and J. Ralph, High Temp. High Pressures **15**, 169 (1983).
[7]J. K. Fink, Int. J. Thermophys. **3**, 165 (1982).
[8]K. Clausen, W. Hayes, J. E. Macdonald, R. Osborn, and M. T. Hutchings, Phys. Rev. Lett. **52**, 1238 (1984).
[9]M. T. Hutchings, J. Chem. Soc., Faraday Trans. II **83**, 1083 (1987).
[10]H. U. Rahman and W. A. Runciman, J. Phys. Chem. Solids **27**, 1833 (1966).
[11]S. Kern, C.-K. Loong, and G. H. Lander, Phys. Rev. B **32**, 3051 (1985).
[12]P. Burlet, J. Rossat-Mignod, S. Quezel, O. Vogt, J. C. Spirlet, and J. Rebizant, J. Less-Common Met. **121**, 121 (1986).
[13]R. Osborn, B. C. Boland, Z. A. Bowden, A. D. Taylor, M. A. Hackett, W. Hayes, and M. T. Hutchings, J. Chem. Soc., Faraday Trans. II **83**, 1105 (1987).
[14]R. Osborn, A. D. Taylor, Z. A. Bowden, M. A. Hackett, W. Hayes, M. T. Hutchings, G. Amoretti, R. Caciuffo, A. Blaise, and J. M. Fournier, J. Phys. C **21**, L931 (1988).
[15]P. G. deGennes, in *Magnetism,* edited by G. T. Rado and H. Suhl (Academic, New York, 1963), Vol. III, p. 115.
[16]A. D. Taylor, B. C. Boland, Z. A. Bowden, and T. J. L. Jones, Rutherford Appleton Laboratory Report No. RAL-87-012, 1987 (unpublished).
[17]W. T. Carnall and H. M. Crosswhite, Argonne National Laboratory Report ANL-84-90, 1985 (unpublished).
[18]R. A. Satten and J. S. Margolis, J. Chem. Phys. **32**, 573 (1960);

33, 618(E) (1960).
[19]M. T. Hutchings, in *Solid State Physics,* edited by F. Seitz and D. Turnbull (Academic, New York, 1964), Vol. 16, p. 227.
[20]K. R. Lea, M. J. M. Leask, and W. P. Wolf, J. Phys. Chem. Solids **23**, 1381 (1962).
[21]C. J. Lenander, Phys. Rev. **130**, 1033 (1963).
[22]J. P. Desclaux and A. J. Freeman, J. Magn. Magn. Mater. **8**, 119 (1978).
[23]G. Amoretti, Commission of the European Communities, Direction Genérale XII, Activity Reports, 1983 (unpublished).
[24]D. J. Newman, Adv. Phys. **20**, 197 (1971).
[25]J. B. Gruber and E. R. Menzel, J. Chem. Phys. **50**, 3772 (1969).
[26]S. J. Allen, Phys. Rev. **166**, 530 (1968); **167**, 492 (1968).
[27]F. Gronvold, N. J. Kveseth, A. Sveen, and J. Tichy, J. Chem. Thermodyn. **2**, 665 (1970); J. J. Huntzicker and E. F. Westrum, *ibid.* **3**, 61 (1971).
[28]G. Dolling, R. A. Cowley, and A. D. B. Woods, Can. J. Phys. **43**, 1397 (1965).
[29]K. Clausen, W. Hayes, J. E. Macdonald, R. Osborn, P. G. Schnabel, M. T. Hutchings, and A. Magerl, J. Chem. Soc., Faraday Trans. II **83**, 1109 (1987).
[30]G. Amoretti, J. Phys. (Paris) **45**, 1067 (1984).
[31]P. Giannozzi and P. Erdös, J. Magn. Magn. Mater. **67**, 75 (1987).
[32]P. Giannozzi, Ph.D. thesis, University of Lausanne, Lausanne, Switzerland, 1988.
[33]G. Solt and P. Erdös, Phys. Rev. B **22**, 4718 (1980).
[34]H. H. Chen and P. M. Levy, Phys. Rev. B **7**, 4267 (1972); **7**, 4284 (1972).
[35]K. Sasaki and Y. Obata, J. Phys. Soc. Jpn. **28**, 1157 (1970).
[36]O. G. Brandt and C. T. Walker, Phys. Rev. **170**, 528 (1968).
[37]D. J. Newman, Austr. J. Phys. **30**, 315 (1977).
[38]G. Amoretti, A. Blaise, J. M. Fournier, R. Caciuffo, J. Larroque, R. Osborn, A. D. Taylor, and Z. A. Bowden, J. Magn. Magn. Mater. **77&78**, 432 (1988).
[39]G. Amoretti, A. Blaise, J. M. Collard, R. O. A. Hall, M. J. Mortimer, and R. Troć, J. Magn. Magn. Mater. **46**, 57 (1984).
[40]S. Nasu, Jpn. J. Appl. Phys. **5**, 1001 (1966).